Stratum corneum occlusion induces water transformation towards lower bonding state: a molecular level *in vivo* study by confocal Raman microspectroscopy

C. Choe*, J. Schleusener[†], S. Choe*, J. Ri*, J. Lademann[†] and M. E. Darvin[†]   iD

*Kim Il Sung University, Taesong District, Ryongnam-Dong, Pyongyang, DPR Korea and [†]Department of Dermatology, Venerology and Allergology, Center of Experimental and Applied Cutaneous Physiology, Charité – Universitätsmedizin Berlin, Corporate Member of Freie Universität Berlin, Humboldt-Universität zu Berlin, Berlin Institute of Health, Charitéplatz 1, Berlin 10117, Germany

Abstract

OBJECTIVE: It is conventionally understood that occlusive effects are the retention of excessive water in the stratum corneum (SC), the increase of SC thickness (swelling) and a decrease of the transepidermal water loss. However, the influence of occlusion on water binding properties in the SC is unknown.

METHODS: The action of plant-derived jojoba and almond oils, as well as mineral-derived paraffin oil and petrolatum topically applied on human skin, is investigated *in vivo* using confocal Raman microspectroscopy. To understand the oils' influence on the SC on the molecular level, the depth-dependent hydrogen bonding states of water in the SC and their relationship to the conformation of keratin, concentration of natural moisturizing factor (NMF) molecules and lipid organization were investigated.

RESULTS: A significant SC swelling was observed only in petrolatum-treated skin. The water concentration was increased in oil-treated skin in the intermediate SC region (40–70% SC depth). Meanwhile, the amount of free, weakly and tightly bound water increased, and strongly bound water decreased in the uppermost SC region (0–30% SC depth). The NMF concentration of oil-treated skin was significantly lower at 50–70% SC depth. The lateral organization of lipids in oil-treated skin was lower at 0–30% SC depth. The secondary structure of keratin was changed towards an increase of β-sheet content in mineral-derived oil-treated skin and changed towards an increase of α-helix content in plant-derived oil-treated skin.

CONCLUSION: The occlusive properties can be summarized as the increase of free water and the transformation of water from a more strongly to a more weakly hydrogen bonding state in the uppermost SC, although some oils cause insignificant changes of the SC thickness. The accompanied changes in the keratin conformation at the intermediate swelling region of the SC also emphasize the role of keratin in the SC's water-transporting system, that is the water in the SC transports intercellularly and intracellularly in the intermediate swelling region and only intercellularly in the uppermost non-swelling region. Bearing this in mind, almond, jojoba and paraffin oils, which are not occlusive from the conventional viewpoint, have an occlusion effect similar to petrolatum on the SC.

Résumé

OBJECTIF: Il est généralement entendu que les effets occlusifs consistent en la rétention d'un excès d'eau dans la couche cornée (stratum corneum, SC), l'augmentation d'épaisseur de la SC (gonflement) et une diminution de la perte d'eau trans-épidermique. Cependant, l'influence de l'occlusion sur les propriétés de fixation de l'eau dans le SC est inconnue.

MÉTHODES: L'action des huiles de jojoba et d'amande d'origine végétale, ainsi que des huiles de paraffine et de pétrolatum d'origine minérale appliquées topiquement sur la peau humaine est *étudiée in vivo* à l'aide de la microspectroscopie Raman confocale. Pour comprendre l'influence des huiles sur le SC au niveau moléculaire, on a étudié les états de liaison hydrogène de l'eau dans le SC en fonction de la profondeur et leur relation avec la conformation de la kératine, la concentration des molécules du facteur naturel d'hydratation (NMF) et l'organisation des lipides.

RÉSULTATS: Un gonflement significatif de le SC n'a été observé que dans la peau traitée au pétrolatum. La concentration en eau a été augmentée dans la peau traitée au pétrolatum dans la région SC intermédiaire (40-70% de profondeur du SC). En meme temps, la quantité d'eau libre, faiblement et fortement liée augmentait, tandis que l'eau fortement liée diminuait dans la région SC supérieure (0-30% de profondeur du SC). La concentration en NMF de la peau traitée à l'huile était plus basse d'une manière significative à 50-70% de profondeur du SC. L'organisation latérale des lipides dans la peau huilée était plus basse à une profondeur du SC de 0 à 30 %. La structure secondaire de la kératine a été modifiée pour augmenter la teneur en feuillet-β dans les peaux huilées d'origine minérale et pour augmenter la teneur en hélice α dans les peaux huilées d'origine végétale.

CONCLUSION: Les propriétés occlusives peuvent être résumées comme l'augmentation de l'eau libre et la transformation de l'eau d'un état de liaison hydrogène plus fort à un état de liaison hydrogène plus faible dans le SC supérieure, bien que certaines huiles provoquent des changements insignifiants de l'épaisseur de la SC.

Correspondence: Maxim E. Darvin, Department of Dermatology, Venerology and Allergology, Center of Experimental and Applied Cutaneous Physiology, Charité – Universitätsmedizin Berlin, Corporate Member of Freie Universität Berlin, Humboldt-Universität zu Berlin, and Berlin Institute of Health, Charitéplatz 1, 10117 Berlin, Germany. Tel.: +49 30 450 518 125; Fax: +49 30 450 518 918; E-mail: maxim.darvin@charite.de

Les modifications de la conformation de la kératine dans la zone de gonflement intermédiaire du SC soulignent également le rôle de la kératine dans le système de transport de l'eau du SC, c'est-à-dire que l'eau est transportée du SC de manière intercellulaire et intracellulaire dans la zone de gonflement intermédiaire et seulement de manière intercellulaire dans la zone non gonflée la plus élevée. En considérant cela, les huiles d'amande, de jojoba et de paraffine, qui ne sont pas occlusives du point de vue conventionnel, ont un effet d'occlusion similaire à celui du pétrolatum sur le SC.

Introduction

Oils, which are lipophilic moisturizers, are the ubiquitous components in cosmetics [1, 2] and medicine [3, 4]. They are used as a base material of creams and ointments for treatment of 'dry skin', one of the common symptoms in dermatology [5]. Oils cause a prominent reduction of the transepidermal water loss (TEWL) due to the film formation [6] and skin surface occlusion and skin barrier enhancements [7, 8] and, thus, increase the water concentration in the stratum corneum (SC) that gives rise to thickening of corneocytes, known as a swelling effect. For instance, topical application of petrolatum increases the SC thickness by ≈32% and decreases the TEWL [8-10], while paraffin and plant-derived oils, as for example almond and jojoba oils, showed modest (10–20%) [10] or no swelling effects [9] and no changes in TEWL [8]. Until now, it has been accepted that oils have several influences on the skin, as for example a moisturizing effect [5] and lipid modulations and complements [11-13]. However, in the literature their mechanisms on the skin barrier function have been controversially discussed [8-10, 12, 14-16].

One opinion is that oils remain only in the uppermost SC region and act as an impermeable membrane [8, 15, 16]. Using confocal laser scanning microscopy, Patzelt et al. [8] showed that the fluorescence dye curcumin, which had been added to the oils, was observed not deeper than in the two uppermost layers of corneocytes. Choe et al. [15, 16] also proved that the penetration depth of petrolatum did not exceed 7 μm (approx. 35% of the SC thickness) by confocal Raman microspectroscopy (CRM), and none of the oils did overcome the skin barrier [9].

Another opinion is that oils, for example petrolatum, do not act as an epicutaneous impermeable membrane, but rather permeate through the SC interstices, allowing normal barrier recovery [10, 14, 17].

The total occlusion and related excessive accumulation of water in the SC is often considered to harm the skin barrier function by causing the destruction of lamellas/ultrastructure of SC lipids [18, 19], prevention of lipid organization recovery [20], widening the intercellular space [21] and bleaching of the skin colour [22]. However, in some cases, occlusion is intended in therapeutic treatment of skin dysfunctions caused by dry environments [23, 24].

Recently, our group found that, despite of petrolatum inducing more SC swelling than plant-derived oils [8, 12], petrolatum-treated skin exhibited more ameliorative ordering of intercellular lipids (ICL) than skin treated with plant-derived oils [12]. This might imply that the oils' occlusive effects go beyond mere swelling of SC or changes of the TEWL.

It was also reported that the water in the SC can be categorized into four types, according to the strength of its hydrogen bonds with the neighbouring molecules, that is single donor–double acceptor (DAA, tightly bound water), double donor–double acceptor (DDAA, strongly bound water), single donor–single acceptor (DA, weakly bound water) and free water [25]. Hereby, the question arises, whether these four water types will simultaneously increase after oil application, as assumed in total occlusion, or accumulate differently. Furthermore, the application of paraffin and plant-derived oils neither changed the TEWL nor swelling [8, 9], which underpins these differences, in terms of water, keratin and lipids.

Solving these problems will not only provide new insights into understanding the occlusive effect induced by oils, but also improve the understanding of the moisturizing effect maintained by creams and ointments. In this study, the depth profiles of the SC's parameters, like water types, depending on the strength of hydrogen bonds, lipid organization and the conformation of keratin [25, 26] in oil-treated skin are investigated non-invasively and in vivo using CRM.

Materials and methods

Applied substances

Four oils were used in this in vivo study, plant-derived jojoba oil (cold-pressed; Henry Lamotte, Bremen, Germany, FFA value = 0.20) and almond oil (Afruse SL, Tarragona, Spain, FFA value = 0.28), mineral-derived paraffin oil (Marcol 82tm; Esso SAF, Rueil-Malmaison, France) and petrolatum (Fagron GmbH & Co.KG, Barsbüttel, Germany). The Raman spectra of the applied oils are presented in Fig. 1 in the fingerprint (a) and high wavenumber region (b) in comparison with a Raman spectrum of the human stratum corneum in vivo (depth 4 μm).

Volunteers

Six healthy volunteers (three female, three male) aged between 23 and 62 years (average 37 years old) participated in this study. The volunteers were instructed not to utilize any skincare products on the forearms at least 72 h and not to bath or shower at least 4 h before the beginning of the experiments. After an acclimation time of 20 min, four 2×2 cm^2 areas were marked on the volar forearms (2 areas on each arm) using a rubber barrier. An amount of 2 mg cm^{-2} of oil was topically applied to one marked area of the forearm and homogenously distributed with soft rubber gloves. Then, every volunteer was subjected to control measurements, scanning the untreated skin areas at 10 measuring points by CRM. Sixty minutes post-oil application, the remaining oil was removed by soft filter paper and more than 10 points for each oil-treated area were measured using CRM. Approval for the measurements had been obtained from the Ethics Committee of the Charité – Universitätsmedizin Berlin, and all procedures complied with the Declaration of Helsinki.

Confocal Raman microspectroscopy

Measurements were performed with an in vivo/ex vivo confocal Raman microscope (Model 3510, RiverD International B.V., Rotterdam, The Netherlands) at 785 nm excitation for acquisition in the fingerprint region (FP, 400–2000 cm^{-1}, exposure time 5 s, 20 mW) and at 671 nm excitation for acquisition in the high wavenumber region (HWN, 2000–4000 cm^{-1}, exposure time 1 s, 17 mW) with a spatial resolution < 5 μm and a spectral resolution < 2 cm^{-1} [27, 28]. The applied light doses are considered to be safe and uncritical for measurements on human skin due to the
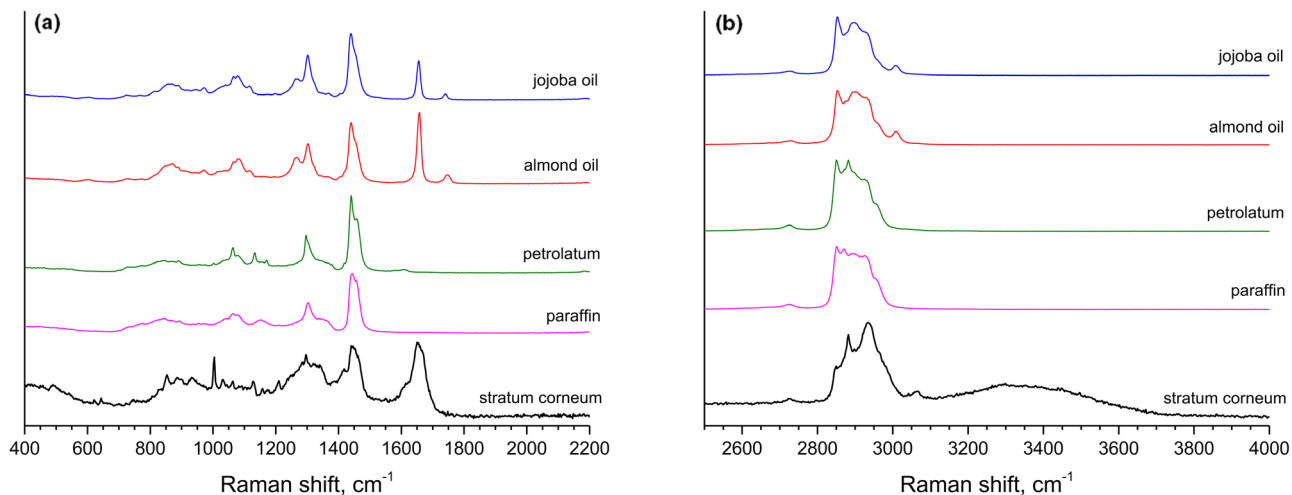
Figure 1 Offset Raman spectra of petrolatum (green line), paraffin (magenta line), jojoba oil (blue line) and almond oil (red line) and *in vivo* human SC at 4 μm depth (black line) in the fingerprint (a) and high wavenumber (b) regions. Raman intensities of all oils are divided by 5.

low local temperature increase of max. 2 °C [29] and the low amount of free radicals generated [30, 31]. Depth- and dose-dependent fluorescence photobleaching does not influence the Raman peak intensities [32], which ensures comparable results. Raman spectra in the FP and HWN regions were acquired at the same positions at 2 μm increments between the position of approx. 10 μm above the surface and 30 μm below the surface, thus ensuring to measure the entire SC.

Data analysis

SC surface and thickness
The skin surface position was determined by the depth profile of the Amide I band at 1650 cm^{-1}, taking the oil contributions into account, as described elsewhere [33]. For the treatment with plant-derived oils, the skin surface points are determined by the peak intensity of the 1003 cm^{-1} band, which was not superimposed by the oils' Raman spectra and produced identical results as the method using the Amide I band. Thereby, the skin surface was determined to be at the position with 50% of the maximum Raman peak intensity from outside of the skin. As the oils only penetrate 8–11 μm in the SC, they do not reach the viable cells of the stratum spinosum. Thus, there is no influence of oils on setting the boundary between the SC and the stratum granulosum (SG). Therefore, the boundary between the SC and the SG can be correctly determined by the water gradient 0.5, which gives comparable results with other SC thickness calculating methods [34].

Water mass percentage and the hydrogen bonding state of water molecules
The newly proposed extended method was applied for the determination of the water concentration in the SC of oil-treated skin [33]. This method is based on the calculation of the O–H Raman band (3350–3550 cm^{-1}) to the Amide I band (1650 cm^{-1}) ratio, which is free of artefacts caused by superposition of skin and oil-based Raman spectra [35].

The Raman spectra in the HWN region were baseline subtracted and decomposed into 10 Gaussian functions, related to lipids ($\approx$2850 cm^{-1} and $\approx$2880 cm^{-1}), keratin ($\approx$2930 cm^{-1}, $\approx$2980 cm^{-1}, $\approx$3060 cm^{-1} and $\approx$3330 cm^{-1}) [22,36,37] and water ($\approx$3005 cm^{-1} – tightly bound water, single donor–double acceptor, DAA; $\approx$3260 cm^{-1} – strongly bound water, double donor–double acceptor, DDAA; $\approx$3450 cm^{-1} – weakly bound water, single donor–single acceptor, DA; and $\approx$3600 cm^{-1} – free water, double donor–single acceptor, DDA and unbound water), as described elsewhere [36-39]. DDAA-bound water has four hydrogen bonds with the surrounding molecules, which constitutes first monolayers of water with surrounding intrinsic components of the SC [40]. DA-bound water has only two hydrogen bonds. It is also known 'partially bound' water [40] and is bound to DDAA-bound water. The hydrogen bonding state of water in the SC is determined as the weakly bound/strongly bound water type ratio [25].

Normalization of the SC depth
The direct comparison of the physiological properties of the SC expressed in absolute depths is not useful, as the SC thickness varies interindividually and between different body sites. Therefore, similar to previous studies [12, 17, 26, 41], the SC depth was normalized to its total thickness and is presented in % of SC depth, based on the assumption that the skin physiological properties are scaled to its SC thickness. However, this normalization process is valid only for untreated skin and causes problems in case of skin treatment with occluding substances, such as oils, which induce non-uniform SC swelling [42, 43]. It should be noted that the 'keratin–water' interaction is responsible for swelling of corneocytes in the SC [44]. The non-uniform swelling was previously shown *ex vivo* using cryo-scanning electron microscopy [43] and *in vivo* using CRM [26]. These studies showed that in relation to swelling, the SC could be separated into three independent regions. In the uppermost region (0–30% SC thickness), the keratin filaments are highly folded, have the least binding sites for water molecules and are referred to as uppermost non-swelling SC region. In the intermediate region (30–70% SC thickness), the water molecules have

the most binding sites. Therefore, this region is most swelled and is called intermediate swelling SC region. In the bottom region (80–100% SC thickness), few water binding sites in keratin filaments exist and, therefore, this region is referred to as bottom low-swelling SC region.

Considering the above-mentioned factors, normalization of the SC depth to its thickness, as previously used [12, 17, 26, 41], does not take the non-uniform swelling of the SC in oil-treated skin into account. To model the non-uniform swelling and compare the skin physiological parameters between untreated and oil-treated skin, the following is hypothesized:

First, there are no changes in the thickness of the uppermost non-swelling and bottom low-swelling SC regions between untreated and oil-treated skin. Second, the changes in the SC thickness of oil-treated skin are only due to the swelling of the intermediate swelling SC region.

The uppermost non-swelling and bottom low-swelling SC region thicknesses in oil-treated skin are calculated from untreated skin. Then, the intermediate swelling SC region thickness in oil-treated skin is calculated by subtracting the uppermost non-swelling and bottom low-swelling SC region thicknesses from the total SC thickness and the ratio of the intermediate swelling SC region thickness between oil-treated and untreated skin is calculated. Thereby, the SC depth in the intermediate swelling SC region of oil-treated skin is scaled down, so that the total scaled thickness of oil-treated skin is identical to untreated SC. Finally, by using the SC thickness of untreated skin, the SC depths of both untreated and oil-treated skin are normalized and presented in the range of 0–100%, which makes it possible to directly compare the SC's physiological parameters of oil-treated and untreated skin.

Lamellar/lateral organization of intercellular lipids
The lamellar packing organization of ICL was determined by calculating the $I_{1080}/(I_{1060} + I_{1130})$ Raman peak intensity ratio, characterizing its *gauche–trans* conformation. The lateral packing organization of ICL was determined by calculating the I_{2880}/I_{2850} Raman peak intensity ratio with exclusion of the keratin contribution. The detailed procedure was recently presented by our group [45].

Concentration of NMF
The depth profiles of the NMF concentration are obtained using the 'SkinTools 2.0' software provided by RiverD International B.V. [46], which is based on linear regression of reference spectra of various skin components (keratin, lactic acid at pH4, urea, trans-urocanic acid at pH4 and pH8, ceramide type III, cholesterol and water), and spectra related to the optical components of the CRM. The NMF concentration was determined as a combination of the pyrrolidone carboxylic acid, ornithine, serine, proline, glycine, histidine at pH4 and pH7 and alanine concentrations [47].

Hereby, the depth profiles of NMF are normalized taking the non-homogeneous distribution of keratin in the SC into account, which is described in detail elsewhere [48].

Secondary structure of keratin
The Amide I band (1580–1720 cm^{-1}) contains information about the secondary structure of keratin. The Raman peak at 1655 cm^{-1} characterizes the α-helix keratin, while the peak at 1670 cm^{-1} corresponds to β-sheet keratin [49,50]. The keratin of the SC is normally arranged in α-helical stable conformation [36]. To analyse the β-sheet/α-helix ratio, a decomposition of the 1580–1720 cm^{-1} range using four Gaussian functions, similar

as presented in [40], was performed. The band centred at 1617 cm^{-1} is assigned to aromatic vibrations of phenylalanine, tyrosine and tryptophan [51, 52]. The band at 1655 cm^{-1} is assigned to α-helix and the band at 1670 cm^{-1} to the β-sheet conformation, and the band at 1685 cm^{-1} is related to turns and random coils of keratin [51, 53]. As the turns and random coils of keratin represent the disordered states, their relative ratio to the α-helix keratin, that is the $(I_{1670} + I_{1685})/I_{1655}$ ratio indicates the ordering regarding the secondary structure of keratin as described elsewhere [26].

Folding properties of keratin
Asymmetric CH$_3$ vibrations are characterized by the position of the 2930 cm^{-1} Raman band. A shift of the maximum position towards lower wavenumbers was shown to be related to the increasing amount of folded proteins regarding the tertiary properties of the keratin filaments [54].

Stability of disulphide bonds in the keratin framework
The most important side-chain reactions of keratin chains are disulphide bonds, and their stability is an important factor for the formation of folded keratin chains [55]. The conformational order of the disulphide bond properties of keratin is calculated in the 474–578 cm^{-1} region, associated with –C–S–S–C– bond vibrations. The 492 cm^{-1} band is associated with the *gauche–gauche–gauche* conformations and the 525 cm^{-1} and 546 cm^{-1} bands correspond to the *gauche–gauche–trans* and *trans–gauche–trans* conformations [49, 55]. The *gauche–gauche–gauche* is the most stable conformation. Therefore, the (*gauche–gauche–gauche*)/(*trans–gauche–trans + gauche–gauche–trans + gauche–gauche–gauche*) ratio is considered a criterion for the strength of disulphide bonds and furthermore the stability of folded keratin chains [26].

Cysteine forming disulphide bonds
Not all cysteine molecules take part in the formation of disulphide bonds. The amount of cysteine molecules participating in building the disulphide bonds in keratin can be calculated by the ratio between the total cysteine concentration (amount of C–S groups, characterized by the Raman band at 690–712 cm^{-1}) and the amount of cysteine forming disulphide bonds (amount of SS bonds, characterized by the Raman band at 474–578 cm^{-1}) [26]. In the present study, we have used the inverse ratio.

Buried/exposed tyrosine
Tyrosine has two configurations. The buried tyrosine forms hydrogen bonds with the side chains of keratin resulting in increasing keratin folding and decreasing possibility to bind with water molecules. The exposed tyrosine indicates the unfolded state, which is able to form hydrogen bonds with surrounding molecules, for instance with water. The ratio of Raman band intensities I_{830}/I_{850} indicates the buried/exposed tyrosine ratio [26, 40].

Statistical analysis

Statistical evaluation was performed using the statistic functions of Origin Pro8 and Microsoft Excel. To confirm statistical differences between the means of two groups, the paired *t* test was applied. ANOVA was used to test for statistical differences for skin treated with four different oils. The graphs are presented with the mean values, and standard deviation is not shown for visual clarity. Differences with $P < 0.01$ were denoted 'highly significant' and are

Table 1 The SC thickness (µm) of untreated skin and skin treated with four different oils in µm. The symbol '*' denotes P-values < 0.05, the symbol '**' denotes P-values < 0.01 between oil-treated and untreated skin

Volunteer number	Intact skin	Almond oil-treated skin	Jojoba oil-treated skin	Paraffin-treated skin	Petrolatum-treated skin
1	19.2 ± 1.3	21.5 ± 2.4	18.5 ± 2.1	19.7 ± 2.3	22.0 ± 3.3*
2	25.5 ± 1.6	28.0 ± 2.0	24.0 ± 1.5	25.8 ± 3.6	29.5 ± 2.6**
3	20.0 ± 1.2	21.0 ± 2.4	22.0 ± 3.3	22.0 ± 2.1	24.0 ± 2.5**
4	19.7 ± 1.2	19.0 ± 1.9	19.0 ± 2.7	20.5 ± 2.2	21.5 ± 1.9*
5	23.0 ± 1.4	21.0 ± 2.4	24.5 ± 3.4	23.5 ± 2.2	26.0 ± 1.8*
6	19.0 ± 1.4	22.5 ± 2.6*	22.0 ± 2.8	23.1 ± 3.2*	22.5 ± 2.5*

marked '**', P < 0.05 were denoted 'different' and are marked '*' in the graphs.

Results

SC thickness

Table 1 shows the SC thickness of untreated and oil-treated skin. The SC thickness of skin treated with almond oil, jojoba oil and paraffin is significantly different (P < 0.05) only for volunteer 6, while no significant differences were found for the other volunteers. The SC thickness of petrolatum-treated skin shows a highly significant increase, compared to untreated skin for all volunteers.

Depth profiles of water and NMF

Figure 2a shows the depth profiles of the water concentration in the SC of untreated and oil-treated skin. In the intermediate SC region (40–70% SC depth), the water concentration is higher in oil-treated skin than in untreated skin [33], which supports the findings that the intermediate SC region is responsible for the

swelling of the entire SC and that the upper and bottom SC regions do not swell [26, 43].

The NMF profiles of oil-treated skin are not significantly different from untreated skin in 0–40% and 80–100% SC depth. In 50–70% SC depth, oil-treated skin has significantly lower NMF concentration than untreated skin (P < 0.05; Fig. 2b), which might be the effect of NMF dilution resulting from increasing water in corneocytes.

Water mobility and the hydrogen bonding state of water

The depth profiles of the water mobility depending on the strength of hydrogen bonds (tightly, strongly, weakly bound and free water) are shown in Fig. 3. It is clearly visible that the amount of free water is significantly larger in oil-treated skin than in untreated skin and is largest in petrolatum-treated skin.

As shown in Fig. 3a, the concentration of free water in oil-treated skin is significantly larger than in untreated skin at 0–20% SC depth (for jojoba oil at 10–20% SC depth) (P < 0.05). Petrolatum-treated skin shows a significant difference at 0–30% SC depth from untreated skin (P < 0.05).
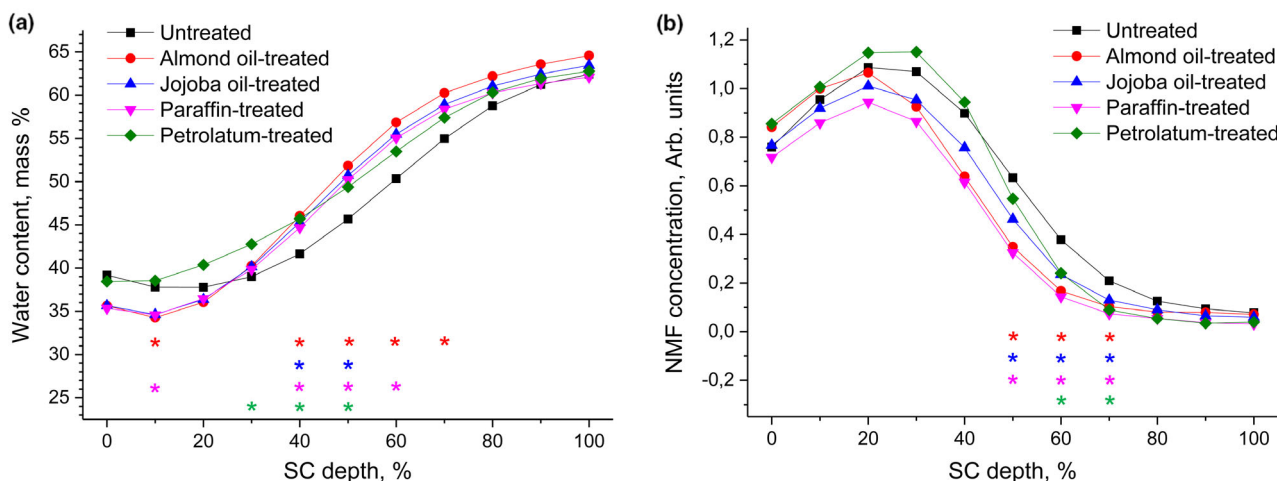

Figure 2 SC depth profiles of the water content (a) and NMF concentration (b) measured *in vivo* in untreated (black squares) and oil-treated human forearm skin (almond oil-treated skin – red circles; jojoba oil-treated skin – blue upward triangles; paraffin-treated skin – magenta downward triangles; petrolatum-treated skin – green diamonds). The SC thickness is normalized taking into consideration the oil-induced SC swelling and non-homogeneous distribution of keratin. '*' represents significant differences P < 0.05 between untreated and oil-treated skin shown with appropriate colour.
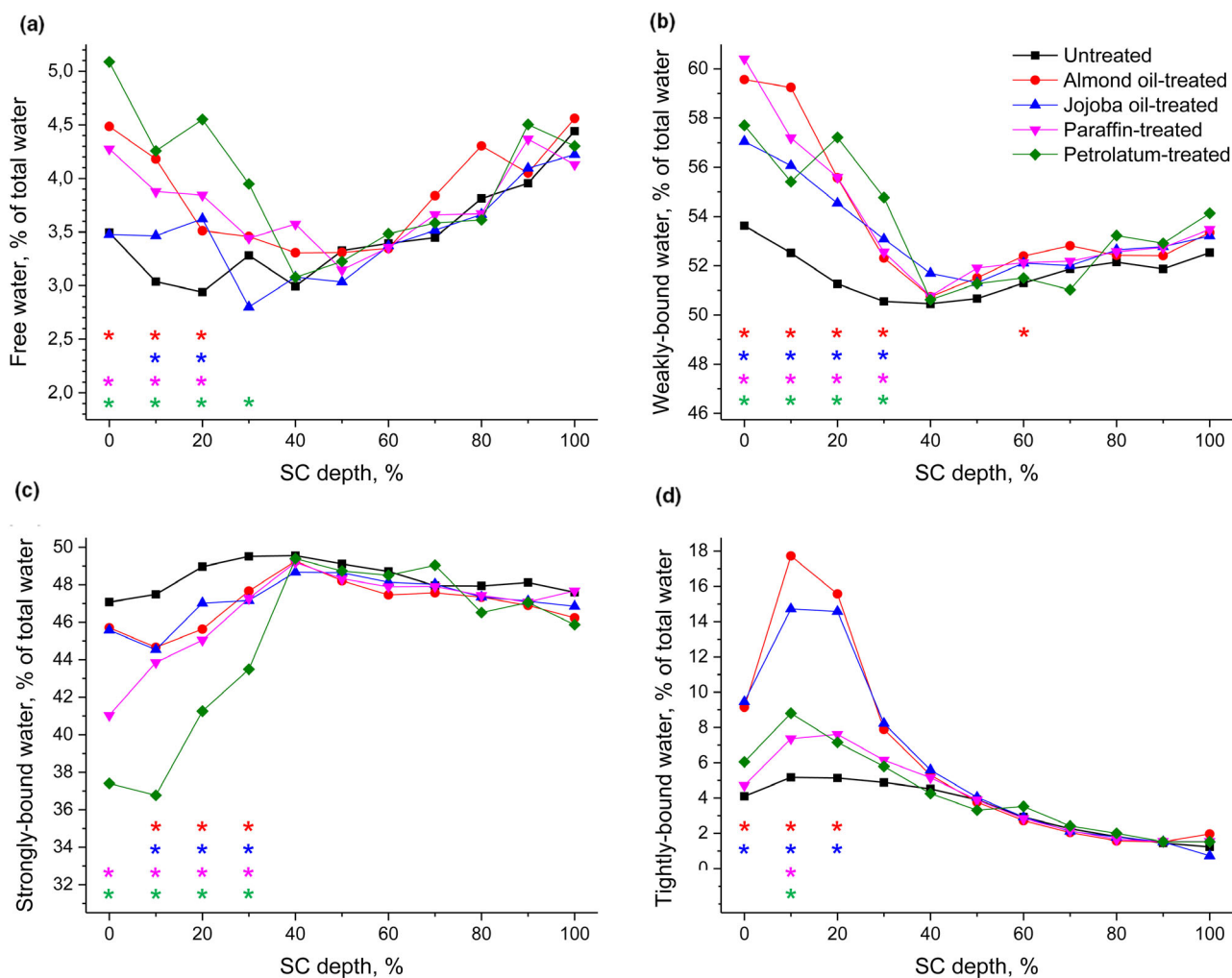
Figure 3 Depth profiles of the concentration of the free (a), weakly bound (b), strongly bound (c) and tightly bound (d) water normalized by the total amount of water measured *in vivo* in untreated (black squares) and oil-treated human forearm skin (almond oil-treated skin – red circles; jojoba oil-treated skin – blue upward triangles; paraffin-treated skin – magenta downward triangles; petrolatum-treated skin – green diamonds). The SC thickness is normalized taking into consideration the oil-induced SC swelling and non-homogeneous distribution of keratin. '*' represents significant difference $P < 0.05$ between untreated and oil-treated skin shown with appropriate colour.

Figure 3b shows a larger concentration of weakly bound water at 0–30% SC depth in oil-treated skin ($P < 0.05$), compared to untreated skin. At the bottom region of the SC, almond oil-treated skin shows significantly higher concentration of weakly bound water at 60% SC depth compared to untreated skin ($P < 0.05$).

Figure 3c shows a lower concentration of strongly bound water at 10–30% SC depth in almond oil-treated and jojoba oil-treated skin ($P < 0.05$) and at 0–30% SC depth in paraffin-treated ($P < 0.05$) and petrolatum-treated skin ($P < 0.01$).

Figure 3d shows a significantly higher concentration of tightly bound water at 0–20% SC depth for almond oil- and jojoba oil-treated skin ($P < 0.05$) and at 20% SC depth for paraffin- and petrolatum-treated skin ($P < 0.05$). Also at 20% SC depth, mineral-derived oil-treated skin has significantly lower tightly bound water than plant-derived oil-treated skin ($P < 0.05$).

Figure 4 shows the depth profiles of the hydrogen bonding state of water in the SC. The application of oils results in a considerable weakening of the hydrogen bonding state of water molecules in the outermost region at 0–30% SC depth ($P < 0.05$ for all four oils). At 40–100% SC depth, skin treated with oils did not show significant differences compared to untreated skin.

The transformation towards a lower hydrogen bonding state of water in petrolatum-treated skin is significantly larger than for almond oil-, jojoba oil- and paraffin-treated skin at 0–30% SC depth ($P < 0.05$).

Intercellular lipid conformation

Figure 5a shows the depth profiles of the lamellar organization of the SC lipids for untreated and oil-treated skin *in vivo* calculated
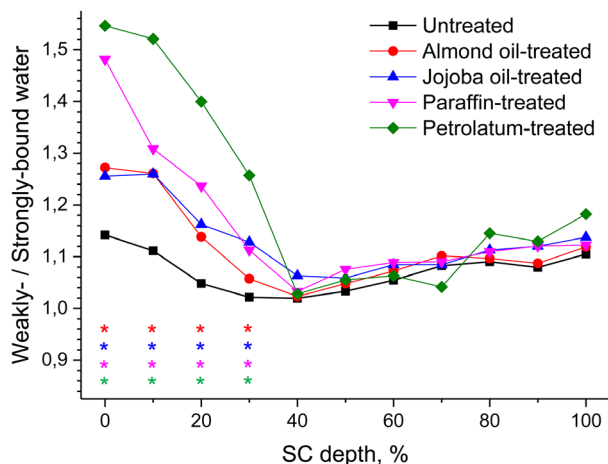
Figure 4 Depth profiles of the hydrogen bonding state of water in the SC measured *in vivo* in untreated (black squares) and oil-treated human forearm skin (almond oil-treated skin – red circles; jojoba oil-treated skin – blue upward triangles; paraffin-treated skin – magenta downward triangles; petrolatum-treated skin – green diamonds). The SC thickness is normalized taking into consideration the oil-induced SC swelling. '*' represents significant difference $P < 0.05$ between untreated and oil-treated skin shown with appropriate colour.

using the swelling-adapted normalization method. At 0–10% of the SC depth, the lamellar packing order of ICL of oil-treated skin is higher than for untreated skin ($P < 0.05$), indicating that the lamellar packing order of SC lipids in oil-treated skin has changed towards a more disordered hexagonal state in comparison to untreated skin. The same tendency is observed at 60–70% for almond oil-treated skin ($P < 0.05$).

Figure 5b shows the depth profiles of the lateral organization of SC lipids for untreated and oil-treated skin *in vivo* calculated using the swelling-adapted normalization method. At 0–30% SC depth, the lateral organization of oil-treated skin is lower than that of untreated skin ($P < 0.05$), indicating that the ICL of oil-treated skin has more low-ordered hexagonal states than that of untreated skin and therefore a reduced skin barrier function. Comparison of the values for oil-treated skin at the regions exceeding 50% SC depth shows that petrolatum-treated skin is closest to untreated skin, while skin treated with other oils tends to have lower values, although no statistical differences were found between oil-treated skin and untreated skin.

Secondary structure of keratin

Figure 6 shows the depth profiles of the secondary structure of keratin determined as the (β–sheet + turns and random coils)/α–helix ratio by decomposition of the Amide I peak at ≈ 1650 cm^{-1}. The plant-derived oils (almond and jojoba oil) show significantly lower values in comparison with untreated skin at 0–30% SC depth ($P < 0.01$ at 0–30% SC depth), which might have been caused by the contribution of pure oils (the inherent value is 0.034 for almond oil and 0.045 for jojoba oil) on the skins' spectrum (see Table 2). Petrolatum-treated skin shows significantly higher values than untreated skin at 0–30, 50–70 and 100% SC depth ($P < 0.05$), while paraffin-treated skin shows significantly higher values only at 50–70% SC depth ($P < 0.05$).

Petrolatum-treated skin shows significantly higher values than almond oil-treated skin (0–100%, $P < 0.01$), jojoba oil-treated skin (0–90%, $P < 0.01$) and paraffin-treated skin (0–20%, $P < 0.05$).
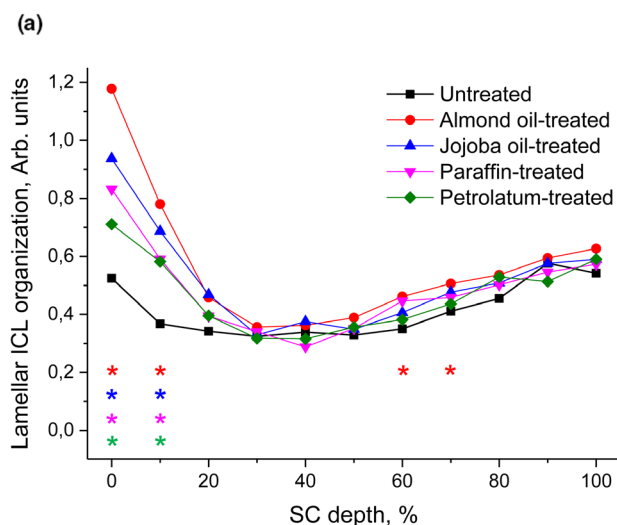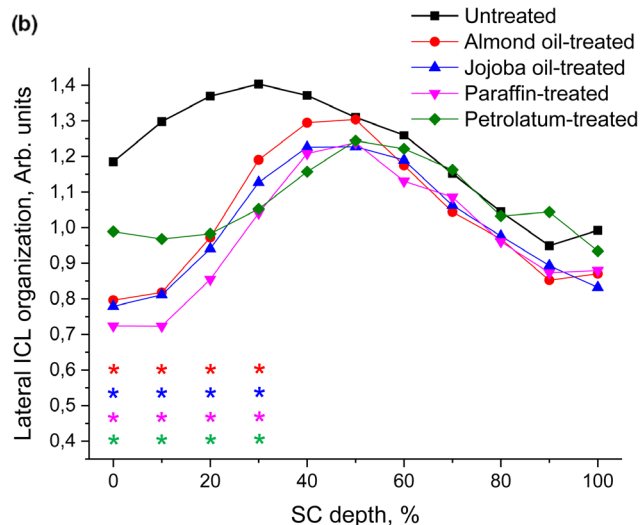

Figure 5 Depth-dependent profiles of the lamellar (a) and the lateral packing order (b) of SC lipids measured *in vivo* in untreated (black squares) and oil-treated human forearm skin (almond oil-treated skin – red circles; jojoba oil-treated skin – blue upward triangles; paraffin-treated skin – magenta downward triangles; petrolatum-treated skin – green diamonds). The SC thickness is normalized taking into consideration the oil-induced SC swelling. '*' represents significant difference $P < 0.05$ between untreated and oil-treated skin shown with appropriate colour.
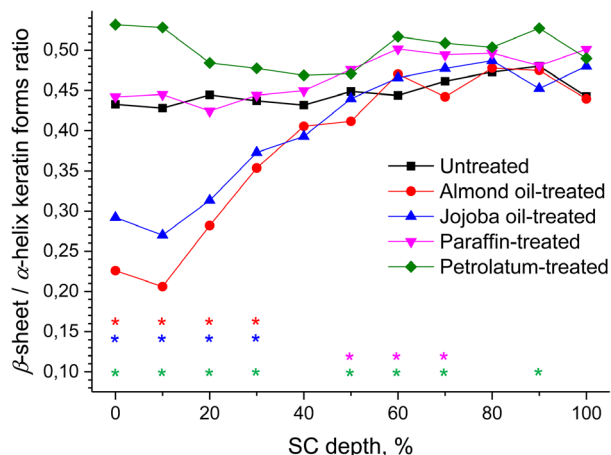
Figure 6 Depth profiles of the secondary structure of keratin measured *in vivo* in untreated (black squares) and oil-treated human forearm skin (almond oil-treated skin – red circles; jojoba oil-treated skin – blue upward triangles; paraffin-treated skin – magenta downward triangles; petrolatum-treated skin – green diamonds). The SC thickness is normalized taking into consideration the oil-induced SC swelling. '*' represents significant differences ($P < 0.05$) between untreated and oil-treated skin shown with appropriate colour.

Paraffin-treated skin has significantly higher values than almond oil- and jojoba oil-treated skin at the 0–60% SC depths ($P < 0.01$).

Tertiary structure of keratin

As shown in Fig. 7a, the stability of disulphide bonds (*gauche-gauche-gauche* (474–508 cm^{-1}) conformation to the total disulphide bond conformations (474–578 cm^{-1})) shows no statistical difference between oil-treated and untreated skin, except for lower petrolatum-treated skin at 10% SC depth ($P < 0.05$), indicating more unstable disulphide bonds in keratin filaments than in untreated skin.

Figure 7b shows that the amount of cysteine molecules involved in the formation of disulphide bonds in keratin filaments. It does not change after application of oils with the exception of almond oil-treated skin showing a lower value at 40% SC depth ($P < 0.05$), that is a smaller amount of disulphide bonds formed by cysteine in keratin filaments, indicating the weakness of interaction between side chains of cysteine in keratin filaments.

Figure 7c shows the depth profiles of buried/exposed tyrosine in oil-treated and untreated skin. Significantly higher values were only found between oil-treated and untreated skin at 70% SC depth ($P < 0.01$ for almond oil- and paraffin-treated skin and $P < 0.05$ for jojoba oil- and petrolatum-treated skin), while the overall tendency is visible for 60–80% SC depth. This means that the tyrosine side chains of keratin transformed into more strongly hydrogen bound state at this exemplary SC depth, which might have been caused by the enhanced amount of water molecules around keratin molecules.

Figure 7d shows the depth-dependent profile of the folding state of keratin determined by the Gaussian peak position at 2930 cm^{-1}, which is significantly lower in oil-treated skin than in untreated skin at 0–40% SC depth ($P < 0.01$). This could be explained by the strong superposition of the oil's and skin Raman spectra at approx. 2930 cm^{-1} (Fig. 1), which is supported by the inherent values of pure oils (lowest value for petrolatum and highest value for almond oil, Table 2). Paraffin-treated skin also shows significantly lower values than almond- and jojoba oil-treated skin (0–10% SC depths, $P < 0.05$). Petrolatum-treated skin shows significantly lower values than for the skin treated with other oils (0–40% SC depths, $P < 0.01$).

Discussion

Effect of oil occlusion on the hydrogen bonding states of water molecules

From Figs 2–4, we postulate that the occlusive effect of oils can be interpreted as the transformation of water molecules towards weaker hydrogen bonding states at the uppermost SC region (0–30% SC depth). Figure 3 shows that free and weakly bound water increased at the outermost SC region in oil-treated skin, but the amount of strongly bound water decreased. An increase of tightly bound water is, probably, an artefact related to the superposition of plant-derived oils- and skin-related Raman bands at approx. 3005 cm^{-1} (see Fig. 1b).

This specific increase of weaker hydrogen bound water (Fig. 3a–b) or transformation towards a weaker hydrogen bonding state of water (Fig. 4) in the uppermost SC regions can be explained by the difference in diffusion coefficients for different hydrogen bound water molecule types, proposed previously [25]. Due to their high mobility, the weakly bound and free water types diffuse faster towards the SC surface than strongly bound water and then accumulate below the impermeable thin layer created by the oils and, as a result, the hydrogen bonding state of water in oil-treated skin

Table 2 Raman features measured on the pure oils and untreated SC. The symbol '–' means absence of Raman contribution

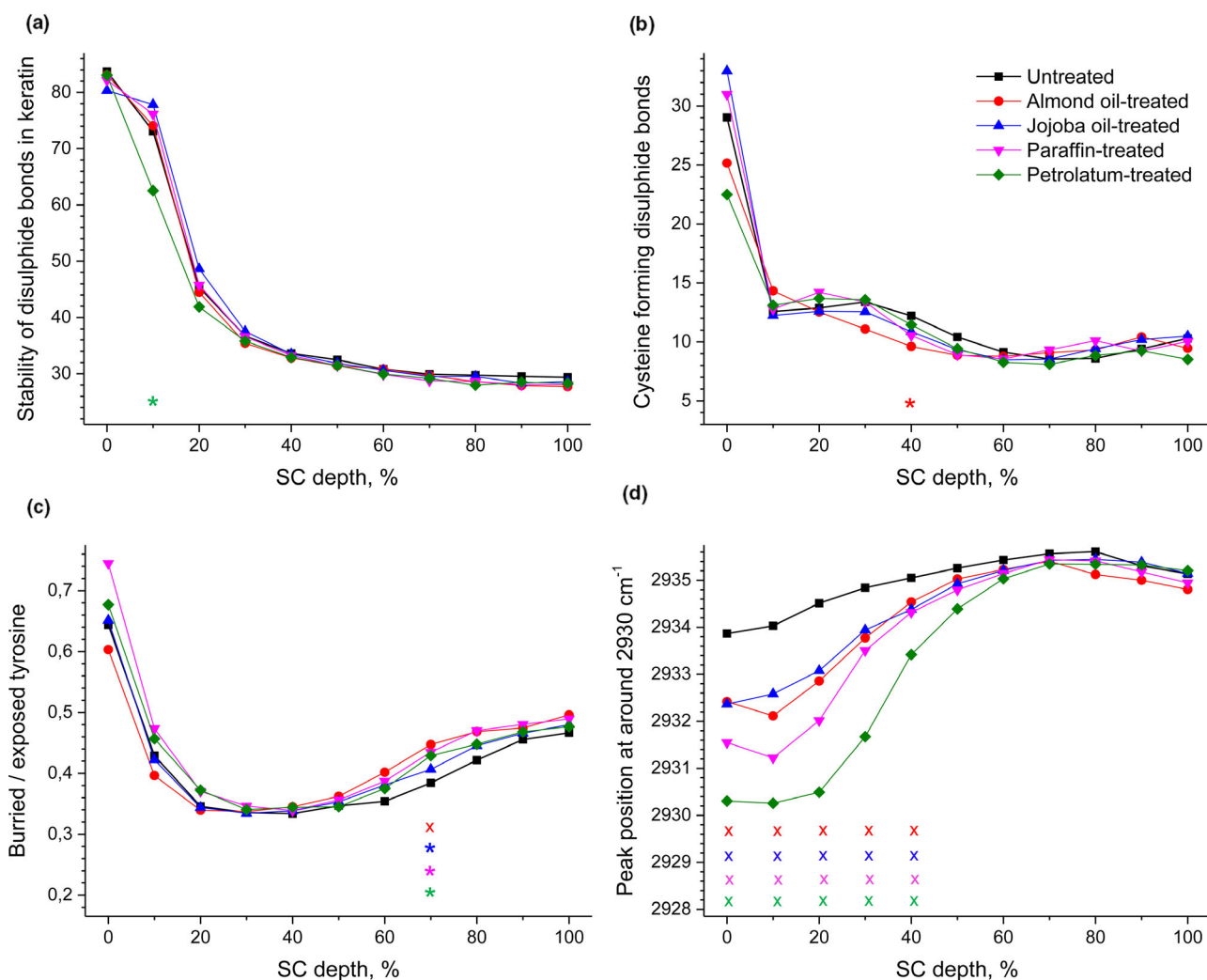|	$I_{1080}/(I_{1130} + I_{1060})$	I_{2880}/I_{2850}	$(I_{1670} + I_{1685})/I_{1655}$	Maximal position around 2930 cm^{-1}
Almond oil	1.26 ± 0.03	0.83 ± 0.01	0.034 ± 0.008	2902 ± 1
Jojoba oil	1.02 ± 0.02	0.76 ± 0.01	0.045 ± 0.006	2896 ± 1
Paraffin oil	0.72 ± 0.03	0.86 ± 0.01	–	2896 ± 1
Petrolatum	0.42 ± 0.11	1.06 ± 0.07	–	2882 ± 1
SC surface	0.53 ± 0.12	1.24 ± 0.17	0.433 ± 0.048	2933.9 ± 0.2
30% SC depth	0.33 ± 0.07	1.45 ± 0.30	0.437 ± 0.027	2934.8 ± 0.2
90% SC depth	0.56 ± 0.08	1.00 ± 0.23	0.480 ± 0.044	2935.3 ± 0.5

Figure 7 Depth profiles of the tertiary structure of keratin filaments in the human SC measured *in vivo* in untreated (black squares) and oil-treated human forearm skin (almond oil-treated skin – red circles; jojoba oil-treated skin – blue upward triangles; paraffin-treated skin – magenta downward triangles; petrolatum-treated skin – green diamonds). The stability of disulphide bonds (a), the amount of cysteine forming disulphide bonds in keratin chains (b), the buried/exposed ratio of tyrosine (c) and the folding states of keratin filaments (d). The SC thickness is normalized taking into consideration the oil-induced SC swelling. '*' and 'X' represent significant ($P < 0.05$) and strongly significant ($P < 0.01$) difference between untreated and oil-treated skin, respectively, shown with appropriate colour.

transforms towards a lower hydrogen bonding state near the skin surface (Fig. 4).

This explanation partly coincides with the results of van Logtestijn *et al.* [17] who showed, without separation for water hydrogen bonding states that oil-treated skin, and especially petrolatum-treated skin, has a higher resistance to water diffusion than untreated skin and its resistance reaches a maximum at the uppermost SC region (approx. 20% SC depth). As shown in Fig. 4, the water transformation towards a lower hydrogen bonding state is larger in petrolatum-treated skin compared to other oils. Considering that the large part of the water diffusion might occur by the weakly bound and free water, this can be explained by the fact that the diffusion of water is more suppressed in petrolatum- treated skin compared to other oils [17].

Effect of oil application on the secondary and tertiary structure of keratin

The oils could affect the Raman spectra of the SC. Table 2 shows the values calculated for pure oils (Fig. 1) and for exemplary depths of untreated SC. The other parameters, for example disulphide bonds (Fig. 7a), cysteine (Fig. 7b) and buried/exposed tyrosine (Fig. 7c), are not influenced by the pure oils' spectra and, therefore, are not shown in Table 2.

At the uppermost SC region, the secondary structure of keratin in petrolatum-treated skin has an apparent transformation from the α-helix towards the β-sheet structure (Fig. 6), which was not observed in paraffin-treated skin. In contrast, in skin treated with plant-derived oils the secondary structure of keratin is transformed towards the α-

helix structure, which is an artefact related to the superposition of the plant-derived oil-related Raman peak at approx. 1655 cm^{-1} on the Raman peak of keratin in the SC (see Fig. 1a and Table 2).

The significantly lower values for plant-derived oils compared to untreated skin are the result of the contribution of plant-derived oils' inherent Raman peak at 1650 cm^{-1}, which superimposes the Amide I band of skin spectra, giving rise to the artifactual decrease of the β-keratin/α-keratin ratio at 0–30% SC depth. As the Raman spectra of mineral oils (paraffin and petrolatum), have no peak around 1650 cm^{-1}, the higher values of petrolatum-treated skin at 0–30% SC depth indicate the transformation of α-helix towards β-sheet keratin, induced by the water due to swelling (increase of weakly bound and free water).

The analysis of the tertiary structure of keratin at the uppermost SC region shows no changes from the viewpoint of side-chain interactions, that is the stability of disulphide bonds (Fig. 7a), the amount of cysteine formed disulphide bonds (Fig. 7b) and the buried/exposed ratio of tyrosine side chains of keratin (Fig. 7c). At the intermediate SC region, more transformation from α-helix to β-sheet keratin is observed in mineral oil-treated skin, but not in plant-derived oil-treated skin. The disulphide side chains of keratin are not changed (Fig. 7a-b), while the tyrosine side chains transformed into more buried states at 70% SC depth in oil-treated skin (Fig. 7c).

At the bottom of the SC (80–100% SC depth), no changes in the tertiary structure/side-chain conformation in keratin filaments were found for oil-treated skin (Fig. 7a–d). Meanwhile, the secondary structure of keratin in petrolatum-treated skin has a higher β-sheet structure (Fig. 6).

These results are in agreement with the findings that corneocytes do not swell equally by the application of oils: intermediately located corneocytes swell more than those located in the upper and bottom SC regions [26,43]. The swelling of corneocytes is accompanied by an increase of the distance between the keratin filaments [56] and also changes the isomerization of keratin filaments in corneocytes. As presented in Fig. 6, the swelling of the SC induced by mineral oils is apparently accompanied by the transformation of keratin from α-helix to β-sheet structure in the intermediate region (50–70% SC depth) and not with side-chain reactions in keratin filaments (Fig. 7). The stronger hydrogen bond interaction of tyrosine or buried states of tyrosine (Fig. 7c) might be related to the prevalence of β-sheet keratin, where the keratin chains are arranged parallel and wider than for the α-helix structure. Thereby, the possibility of forming hydrogen bonds with other keratin chains (interchain bonds) in β-sheet keratin increases, compared with coiled α-helix keratin.

Swelling of corneocytes and water binding with NMF, lipids and keratin

Considering the obtained depth profiles for NMF (Fig. 2b), lipid organization (Fig. 5), the concentration of water depending on the strength of its binding (Fig. 3), the hydrogen bonding state of water (Fig. 4), the secondary structure (Fig. 6) and the tertiary structure of keratin (Fig. 7), the following conclusions about the swelling-induced changes in the SC have been provided:

In the uppermost SC regions (0–30% SC depth), there is no difference in NMF concentration for untreated and oil-treated skin (Fig. 2b). The concentration of free and weakly bound water increases (Fig. 3), while the concentration of strongly bound water and, as a result the hydrogen bonding state of water molecules, decreases (Figs 3 and 4) in oil-treated skin compared to untreated skin. The values vary between the applied oils.

In the previous studies, the concentration of NMF and the removal of mechanical constraints (non-peripheral corneodesmosomes) [57-60] are considered the key factors for the swelling of corneocytes and the hygroscopic NMF molecules are considered the critical biomolecules for binding water [42, 59].

These findings might explain the hydrogen bonding states of water as follows:

The water in the uppermost non-swelling SC region might be mainly in the intercellular space of corneocytes, as in an intercalated phase in the applied oils and ICL of the SC.

The corneocytes transit from 'fragile' to 'rigid' phenotypes as they move towards the surface of the SC [60]. These 'rigid' corneocytes have an increased level of transglutaminase-mediated protein cross-links and envelope-bound ceramides. The strengthened cornified envelopes of corneocytes in the uppermost non-swelling SC region withstand the osmotic effects of NMF and, thus, prevent the water molecules from entering into the corneocytes and also hinder combining the NMF molecules inside the corneocytes with water [61]. This is often observed by cryo-electron microscopy [43] and our results [26]. In addition, the corneocytes get stronger and do not swell at the superficial SC depths [59, 60]. In uppermost non-swelling SC region, the applied oils and the SC lipids consist of hydrophobic environments, which promote the weakly bound hydrogen interactions of water with environmental molecules. Furthermore, the occlusion widens the intercellular space between corneocytes [21] and might create the storage of water in the intercellular space of the SC [19, 62]. As shown in Figs 3 and 4, the water molecules in the uppermost non-swelling SC region of oil-treated skin are in weaker hydrogen bound states. We therefore assume that the water storage might emerge from the oil-treated SC reservoir surrounded by lipophilic substances in the intercellular space.

Compared to untreated skin, the more disordered hexagonal state of intercellular lipids in the uppermost SC depths (Fig. 5) could additionally indicate the widening or a SC reservoir creation inside the intercellular lipid lamellas.

The secondary structure of keratin is changed stronger in mineral oil-treated skin compared to plant oil-treated skin.

The amount of β-sheet keratin in 0–30% and 50–70% SC depth in petrolatum-treated skin provides more possibility for keratin chains to bind water via hydrogen bonds (Fig. 6).

Despite the increase of water concentration at these SC depths (Fig. 2a), the hydrogen bonding states of water do not change at 50–70% SC depth (Fig. 3a–d), although the hygroscopic NMF concentration significantly decreases (Fig. 2b).

The observed hydrogen bonding of water in the intermediate swelling SC region in oil-treated skin can be explained as follows:

If the diffusion path of water, the intercellular lipid space [63] is occluded by the oils in the uppermost non-swelling SC region, it causes a decrease of transepidermal water diffusion. This retention of water could provide the possibility for water that is transported through the intercellular space to penetrate into the corneocytes due to osmotic effect. The mass percentage of water increases in oil-treated skin in the intermediate swelling SC region, for example at 60% SC depth, the presence of a larger amount of β-sheet- than α-helix keratin provides more vacancies to bind water and plays a compensatory role for dilution of NMF by the increasing water concentration and water binding (Fig. 6). Higher swelling of the corneocytes in the intermediate region was also reported by Caussin et al. [43]. At the bottom region (80–100% SC depth), the conformation of keratin and the hydrogen bonding states of water remain unchanged in oil-treated skin, except for petrolatum-treated skin,

which implies that the application of oils usually does not change the corneocytes at these depths.

Regarding the tertiary structure of keratin, it seems that the influence of the oils' occlusion is limited.

Conclusion

In conclusion, our investigations addressed the changes of the depth profiles of the hydrogen bonding states of water in oil-treated skin (almond, jojoba, paraffin and petrolatum). Until now, the understanding of occlusion effects on the SC is the retention of excessive water in the SC, the increase of SC thickness and a decrease of the TEWL. In this study, new concepts of occlusive effects by oils and swelling of the SC were proposed. The occlusive properties might be defined as the increase of free water and the transformation of water from strongly to weakly bound state in the uppermost non-swelling SC region, even if there is no TEWL change in oil-treated skin. The accompanied changes in the keratin conformation in the secondary structure in the intermediate swelling SC region also emphasize the role of keratin in the water-transporting system in the SC, that is the water is stored intracellularly in the intermediate swelling SC region and the secondary structure of keratin might be the hydrogen bonding partner for water. From these viewpoints, almond, jojoba and paraffin oils are not occlusive from the conventional viewpoints, that is do not significantly increase the SC thickness and do not change the TEWL, but in respect of the hydrogen bonding state of water, they have an occlusion effect similar to petrolatum for skin.

Acknowledgements

References

1. Leyden, JL, Rawlings, AV. *Skin moisturization*. Marcel Dekker, New York (2002).

2. Bielfeldt, S., Blaak, J., Laing, S. *et al.* Deposition of plant lipids after single application of a lip care product determined by confocal raman spectroscopy, corneometry and transepidermal water-loss. *Int. J. Cosmet. Sci.* **41**, 281–291 (2019).

3. Sakata, O., Fujii, M., Koizumi, N., Nakade, M., Kameyama, K. and Watanabe, Y. Effects of oils and emulsifiers on the skin penetration of stearyl glycyrrhetinate in oil-in-water emulsions. *Biol. Pharmaceut. Bull.* **37**, 486–489 (2014).

4. Barre, D.E. Potential of evening primrose, borage, black currant, and fungal oils in human health. *Ann. Nutr. Metab.* **45**, 47–57 (2001).

5. Loden, M. Effect of moisturizers on epidermal barrier function. *Clin. Dermatol.* **30**, 286–296 (2012).

6. de Melo, M.O. and Maia Campos P. Application of biophysical and skin imaging techniques to evaluate the film-forming effect of cosmetic formulations. *Int. J. Cosmet. Sci.* **41**, 579–584 (2019).

7. Buraczewska, I., Brostrom, U. and Loden, M. Artificial reduction in transepidermal water loss improves skin barrier function. *Br. J. Dermatol.* **157**, 82–86 (2007).

8. Patzelt, A., Lademann, J., Richter, H. *et al.* In vivo investigations on the penetration of various oils and their influence on the skin barrier. *Skin Res. Technol.* **18**, 364–369 (2012).

9. Choe, C., Lademann, J. and Darvin, M.E. Analysis of human and porcine skin in vivo/ex vivo for penetration of selected oils by confocal Raman microscopy. *Skin Pharmacol. Physiol.* **28**, 318–330 (2015).

10. Stamatas, G.N., de Sterke, J., Hauser, M., von Stetten, O. and van der Pol, A. Lipid uptake and skin occlusion following topical application of oils on adult and infant skin. *J. Dermatol. Sci.* **50**, 135–142 (2008).

11. Gassenmeier, T.B., Bush, P., Hensen, H. Some aspects of refatting the skin: effects oriented to skin lipids for improving skin properties. *Cosmet Toilet.* **113**, 89–92 (1998).

12. Choe, C., Schleusener, J., Lademann, J. and Darvin, M.E. In vivo confocal Raman microscopic determination of depth profiles of the stratum corneum lipid organization influenced by application of various oils. *J. Dermatol. Sci.* **87**, 183–191 (2017).

13. Zhang, Z., Lukic, M., Savic, S. and Lunter, D.J. Reinforcement of barrier function - skin repair formulations to deliver physiological lipids into skin. *Int. J. Cosmet Sci.* **40**, 494–501 (2018).

14. Ghadially, R., Halkiersorensen, L. and Elias, P.M. Effects of petrolatum on stratum-corneum structure and function. *J. Am. Acad. Dermat.* **26**, 387–396 (1992).

15. Choe, C.-S., Lademann, J. and Darvin, M.E. Gaussian-function-based decon. *Laser Phys.* **24**, 105601 (2014).

16. Choe, C., Lademann, J. and Darvin, M.E. Confocal Raman microscopy for investigating the penetration of various oils into the human skin in vivo. *J. Dermatol. Sci.* **79**, 176–178 (2015).

17. van Logtestijn, M.D., Dominguez-Huttinger, E., Stamatas, G.N. and Tanaka, R.J. Resistance to water diffusion in the stratum corneum is depth-dependent. *PLoS One* **10**, e0117292 (2015).

18. Warner, R.R., Boissy, Y.L., Lilly, N.A. *et al.* Water disrupts stratum corneum lipid lamellae: damage is similar to surfactants. *J. Invest. Dermatol.* **113**, 960–966 (1999).

19. Warner, R.R., Stone, K.J. and Boissy, Y.L. Hydration disrupts human stratum corneum ultrastructure. *J. Invest. Dermatol.* **120**, 275–284 (2003).

20. Grubauer, G., Elias, P.M. and Feingold, K.R. Transepidermal water loss: the signal for recovery of barrier structure and function. *J. Lipid Res.* **30**, 323–333 (1989).

21. Lindberg, M., Johannesson, A. and Forslind, B. The effect of occlusive treatment on human skin: an electron microscopic study on epidermal morphology as affected by occlusion and dansyl chloride. *Acta Derm. Venereol.* **62**, 1–5 (1982).

22. Mathias, C.G.T. Prevention of occupational contact-dermatitis. *J. Am. Acad. Dermatol.* **23**, 742–748 (1990).

23. Denda, M. Influence of dry environment on epidermal function. *J. Dermatol. Sci.* **24** (Suppl 1), S22–S28 (2000).

24. Anderson, R.L., Cassidy, J.M., Hansen, J.R. and Yellin, W. The effect of in vivo occlusion on human stratum corneum hydration-dehydration in vitro. *J. Invest. Dermatol.* **61**, 375–379 (1973).

25. Choe, C., Lademann, J. and Darvin, M.E. Depth profiles of hydrogen bound water molecule types and their relation to lipid and protein interaction in the human stratum corneum in vivo. *Analyst* **141**, 6329–6337 (2016).

26. Choe, C., Schleusener, J., Lademann, J. and Darvin, M.E. Keratin-water-NMF interaction as a three layer model in the human stratum corneum using in vivo confocal Raman microscopy. *Sci. Rep.* **7**, 15900 (2017).

27. Caspers, P.J., Lucassen, G.W., Bruining, H.A. and Puppels, G.J. Automated depth-scanning confocal Raman microspectrometer for rapid in vivo determination of water concentration profiles in human skin. *J. Raman Spectroscopy* **31**, 813–818 (2000).

28. Darvin, M.E., Meinke, M.C., Sterry, W. and Lademann, J. Optical methods for noninvasive determination of carotenoids in human and animal skin. *J. Biomed. Opt.* **18**, 61230 (2013).

29. Akhalaya, M.Y., Maksimov, G.V., Rubin, A.B., Lademann, J. and Darvin, M.E. Molecular action mechanisms of solar infrared radiation and heat on human skin. *Ageing Res. Rev.* **16**, 1–11 (2014).

30. Darvin, M.E., Gersonde, I., Albrecht, H., Zastrow, L., Sterry, W. and Lademann, J. In vivo Raman spectroscopic analysis of the influence of IR radiation on the carotenoid antioxidant substances beta-carotene and lycopene in the human skin. Formation of free radicals. *Laser Phys. Lett.* **4**, 318–321 (2007).

31. Robert, C., Bonnet, M., Marques, S., Numa, M. and Doucet, O. Low to moderate doses of infrared A irradiation impair extracellular matrix homeostasis of the skin and contribute to skin photodamage. *Skin Pharmacol. Physiol.* **28**, 196–204 (2015).

32. Schleusener, J., Lademann, J. and Darvin, M.E. Depth-dependent autofluorescence photobleaching using 325, 473, 633, and 785 nm of porcine ear skin ex vivo. *J. Biomed. Opt.* **22**, 091503 (2017).

33. Choe, C., Schleusener, J., Choe, S., Lademann, J. and Darvin, M.E. A modification for the calculation of water depth profiles in oil-treated skin by in vivo confocal Raman microscopy. *J. Biophoton.* **13**, e201960106 (2020).

34. Ri, J.S., Choe, S.H., Schleusener, J., Lademann, J., Choe, C.S. and Darvin, M.E. In vivo tracking of DNA for precise determination of the stratum corneum thickness and superficial microbiome using confocal Raman microscopy. *Skin Pharmacol. Physiol.* **33**, 30–37 (2020).

35. Darvin, M.E., Choe, C., Schleusener, J.. Response to comment by Puppels et al. on "A modification for the calculation of water depth profiles in oil-treated skin by in vivo Raman microscopy". *J. Biophoton.* **13**, e2460. (2020).

36. Gniadecka, M., Faurskov Nielsen, O., Christensen, D.H. and Wulf, H.C. Structure of water, proteins, and lipids in intact human skin, hair, and nail. *J. Invest. Dermatol.* **110**, 393–398 (1998).

37. Sun, Q. The Raman OH stretching bands of liquid water. *Vib. Spectrosc.* **51**, 213–217 (2009).

38. Sun, Q. and Qin, C. Raman OH stretching band of water as an internal standard to determine carbonate concentrations. *Chemical Geol.* **283**, 274–278 (2011).

39. Unal, M. and Akkus, O. Shortwave-infrared Raman spectroscopic classification of water fractions in articular cartilage ex vivo. *J. Biomed. Opt.* **23**, 1–11 (2018).

40. Vyumvuhore, R., Tfayli, A., Duplan, H., Delalleau, A., Manfait, M. and Baillet-Guffroy, A. Effects of atmospheric relative humidity on Stratum Corneum structure at the molecular level: ex vivo Raman spectroscopy analysis. *Analyst* **138**, 4103–4111 (2013).

41. Boireau-Adamezyk, E., Baillet-Guffroy, A. and Stamatas, G.N. Mobility of water molecules in the stratum corneum: effects of age and chronic exposure to the environment. *J. Invest. Dermatol.* **134**, 2046–2049 (2014).

42. Rawlings, A.V. and Harding, C.R. Moisturization and skin barrier function. *Dermatol. Ther.* **17**(s1), 43–48 (2004).

43. Caussin, J., Groenink, H.W., de Graaff, A.M. et al. Lipophilic and hydrophilic moisturizers show different actions on human skin as revealed by cryo scanning electron microscopy. *Exp. Dermatol.* **16**, 891–898 (2007).

44. Norlen, L., Emilson, A. and Forslind, B. Stratum corneum swelling. Biophysical and computer assisted quantitative assessments. *Arch. Dermatol. Res.* **289**, 506–513 (1997).

45. Choe, C., Lademann, J. and Darvin, M.E. A depth-dependent profile of the lipid conformation and lateral packing order of the stratum corneum in vivo measured using Raman microscopy. *Analyst* **141**, 1981–1987 (2016).

46. Caspers, P.J., Lucassen, G.W., Carter, E.A., Bruining, H.A. and Puppels, G.J. In vivo confocal Raman microspectroscopy of the skin: noninvasive determination of molecular concentration profiles. *J. Invest. Dermatol.* **116**, 434–442 (2001).

47. Koppes, S.A., Kemperman, P., Van Tilburg, I. et al. Determination of natural moisturizing factors in the skin: Raman microspectroscopy versus HPLC. *Biomarkers* **22**, 502–507 (2017).

48. Choe, C., Choe, S., Schleusener, J., Lademann, J. and Darvin, M.E. Modified normalization method in in vivo stratum corneum analysis using confocal Raman microscopy to compensate non-homogenous distribution of keratin. *J. Raman Spectroscopy* **50**, 945–957 (2019).

49. Edwards, H.G., Hunt, D.E. and Sibley, M.G. FT-Raman spectroscopic study of keratotic materials: horn, hoof and tortoiseshell.

Spectrochim. Acta A Mol. Biomol. Spectrosc. **54**, 745–757 (1998).

50. Zhang, G., Moore, D.J., Flach, C.R. and Mendelsohn, R. Vibrational microscopy and imaging of skin: from single cells to intact tissue. *Anal. Bioanal. Chem.* **387**, 1591–1599 (2007).

51. Movasaghi, Z., Rehman, S. and Rehman, I.U. Raman spectroscopy of biological tissues. *Appl. Spectroscopy Rev.* **42**, 493–541 (2007).

52. Lefevre, T., Rousseau, M.E. and Pezolet, M. Protein secondary structure and orientation in silk as revealed by Raman spectromicroscopy. *Biophys. J.* **92**, 2885–2895 (2007).

53. Yager P.Membranes. In: *Biological Applications of Raman Spectroscopy* (Spiro, T.G., ed.), pp. 203–61. Wiley, New York (1987).

54. Verma, S.P. and Wallach, D.F.H. Changes of Raman-scattering in CH-stretching regions during thermally induced unfolding of Ribonuclease. *Biochem. Biophys. Res. Commun.* **74**, 473–479 (1977).

55. Akhtar, W. and Edwards, H.G. Fourier-transform Raman spectroscopy of mammalian and avian keratotic biopolymers. *Spectrochim. Acta A Mol. Biomol. Spectrosc.* **53**, 81–90 (1997).

56. Hey, M.J., Taylor, D.J. and Derbyshire, W. Water sorption by human callus. *Biochem. Biophys. Acta.* **540**, 518–533 (1978).

57. Harding, C.R., Watkinson, A., Rawlings, A.V. and Scott, I.R. Dry skin, moisturization and corneodesmolysis. *Int. J. Cosmet. Sci.* **22**, 21–52 (2000).

58. Long, S., Banks, J., Watkinson, A., Harding, C. and Rawlings, A.V. Desmocollin 1: A key marker for desmosome processing in the stratum corneum. *J. Invest. Dermatol.* **106**, 397 (1996).

59. Rawlings, A.V. and Matts, P.J. Stratum corneum moisturization at the molecular level: an update in relation to the dry skin cycle. *J. Invest. Dermatol.* **124**, 1099–1110 (2005).

60. Rawlings, A.V. Recent advances in skin 'barrier' research. *J. Pharm. Pharmacol.* **62**, 671–677 (2010).

61. Harding, C. and Scott, I. Stratum corneum moisturizing factors. In: *Skin Moisturization* (Leyden, J. and Rawlings, A., eds.), pp. 61–80. Marcel Dekker, Inc, New York (2002).

62. van Hal, D.A., Jeremiasse, E., Junginger, H.E., Spies, F. and Bouwstra, J.A. Structure of fully hydrated human stratum corneum: a freeze-fracture electron microscopy study. *J. Invest. Dermatol.* **106**, 89–95 (1996).

63. Kasting, G.B., Barai, N.D., Wang, T.F. and Nitsche, J.M. Mobility of water in human stratum corneum. *J. Pharm. Sci.* **92**, 2326–2340 (2003).